Aftershock Imaging with Dense Arrays (AIDA) Following the M_w 4.0 Waterboro Earthquake of 16 October 2012 Maine, U.S.A.

by Diego A. Quiros, Anastasija Cabolova, Larry D. Brown, Chen Chen, John E. Ebel, and Justin Starr

ABSTRACT

Arrays of highly portable, exploration style seismographs were deployed following the 16 October 2012 M_w 4.0 Waterboro, Maine, earthquake with the goal of improving hypocenter locations and source mechanisms of aftershocks, lowering the detection threshold for such aftershocks, and using the aftershocks as sources to image subsurface structure in the hypocentral volume. Based on the Aftershock Imaging with Dense Arrays (AIDA) experience following the Mineral, Virginia, earthquake of August 2011, the Maine deployment consisted of three complementary arrays totaling 110 stations: one array was for event detection and location, another for structural imaging, and a third for measuring regional attenuation. Although the arrays operated from day 3 through day 10 following the mainshock, only one aftershock was detected by the 43 stations that had been deployed at the time of the event. This aftershock was located at a focal depth of 6.9 ± 0.15 km, with a horizontal uncertainty of ~0.15 km. Although the strike-slip focal mechanism for this aftershock differs from the thrust mechanism of the mainshock, both share an east–west maximum stress direction. Recordings of the aftershock from the high-density portion of the deployment show possible upper- and lower-crustal reflections that we attempt to image using vertical seismic profiling methods. However, the lack of redundant sources and the limited areal extent of the imaging arrays hinders any useful interpretation of the nature of the crustal reflections. Based on comparison with the Virginia experiment, in which numerous aftershocks were recorded, and from examining the signal-to-noise ratio of the single aftershock recorded, we believe the AIDA Maine deployment should have detected any aftershocks greater than magnitude m_b of approximately −2.5. That only one aftershock was detected supports the observation that earthquakes in some intraplate areas are notable for their lack of aftershock activity down to this level.

INTRODUCTION

On 16 October 2012 at approximately 7:12 p.m. (EST), an M_w 4.0 earthquake struck near Waterboro, Maine (U.S. Geological Survey [USGS], 2012). Following this event, a suite of local arrays were deployed around the epicentral region (Fig. 1). These arrays differ from conventional aftershock arrays in that large numbers of highly portable seismographs (REF TEK RT 125A Texans coupled with 4.5 Hz geophones), originally designed for controlled source seismic reflection and refraction experiments, were deployed at relatively close spacing (i.e., ~200 m) as part of the aftershock monitoring effort. This deployment was designed based on experience with a similarly dense deployment (Aftershock Imaging with Dense Arrays [AIDA]) following the 2011 M_w 5.8 Mineral, Virginia, earthquake (Brown *et al.*, 2011; Davenport *et al.*, 2015).

DEPLOYMENT

The Maine AIDA deployment (Fig. 1a) consisted of three complementary arrays totaling 110 seismic stations. The first array deployed was designed to encompass the potential aftershock zone, thus providing adequate azimuthal coverage for accurate event location. It consisted of 20 stations spaced ~5 km apart in a grid (Fig. 1a), a layout similar to a conventional, relatively well-instrumented aftershock array (e.g., Bounif *et al.*, 2004; Kim and Chapman, 2005; Huang *et al.*, 2008). The second array, a high-density array (HDA), consisted of a box grid of 60 stations spaced very close together (i.e., ~200 m) the purpose of which was to record aftershock signals in relatively unaliased form for structural imaging (Fig. 1a). These two arrays used vertical-component 4.5 Hz geophones (Geospace GS-11D) and a single recorder (REF TEK RT 125A Texan) sampling at 100 samples/s. The third array was a profile through the area with 28 three-component (3C) recording stations (4.5 Hz Sercel L-28-3D geophone coupled with three Texans, each programmed to record at a rate of 100 Hz) spaced at 1 km to allow measurement of the regional attenuation of seismic energy (Fig. 1a). In many respects, the Maine AIDA deployment, like the Virginia antecedent, was a small-scale warm up for the much more ambitious requirements of a dense 2D grid needed for true 3D aftershock imaging.

The Maine AIDA experiment recorded continuously for seven days (19 October–25 October 2012), with the

doi: 10.1785/0220140169

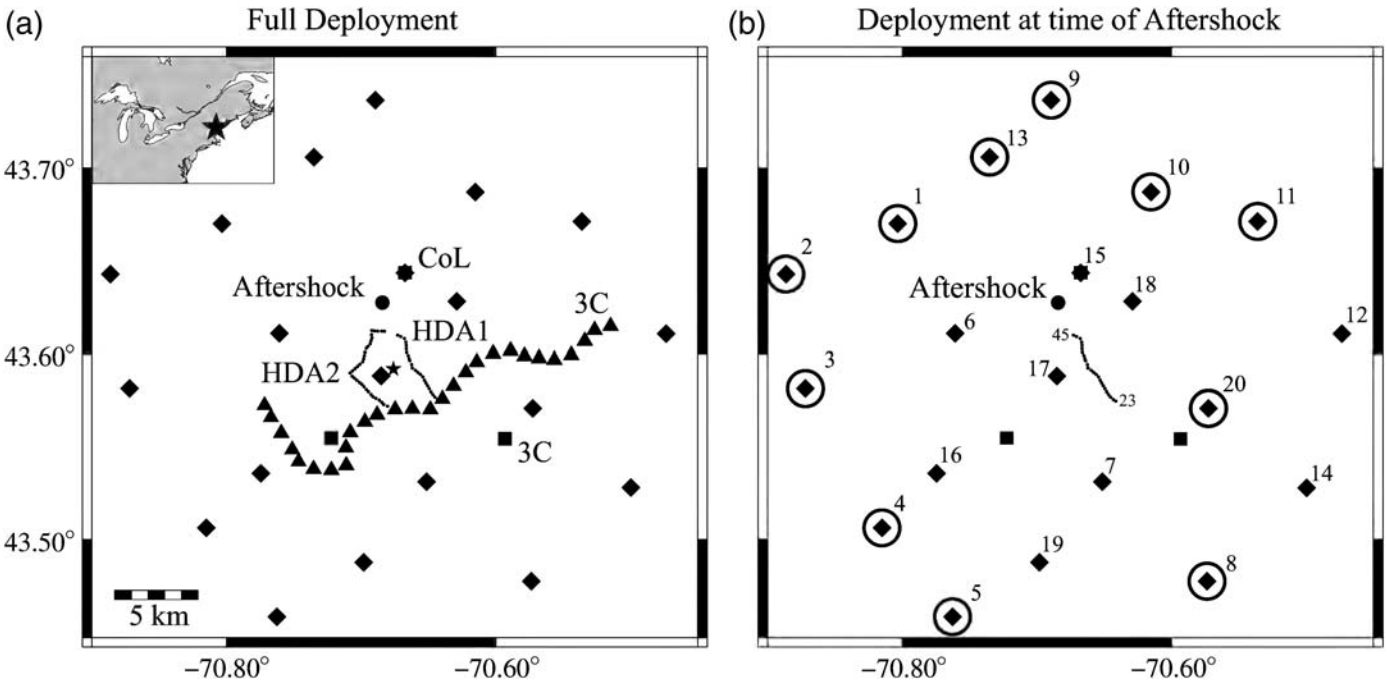

▲ **Figure 1.** Distribution of seismographs near the epicenter of the M_w 4.0 Waterboro, Maine, earthquake. Inset map shows a star centered on the mainshock epicenter. (a) Full deployment of stations around the mainshock epicenter (star), enclosed by the high-density arrays (HDA) (dotted lines), and the three-component (3C) array (triangles). The location array (diamonds) and the three Weston Observatory 3C stations (squares) are shown. (b) Deployment of stations at the time of the aftershock (solid circle). AIDA stations are numbered 1–20 for the location array and 23–45 for the HDA 1 stations (stations 21 and 22 were removed for quality control and did not record the aftershock). The circled diamonds are the subset of the location array stations referred to in the location analysis.

deployment for all three arrays finalized on 21 October. Although the arrays operated from day 3 through day 10 following the mainshock, only one aftershock was detected, occurring on 20 October at 07:46:35.06 ± 0.02 s (UTC). At the time of the aftershock, 43 AIDA stations had been deployed (Fig. 1b).

In addition to the AIDA experiment, Weston Observatory of Boston College deployed three seismic stations for aftershock monitoring (Fig. 1b). Each of the Weston Observatory portable seismic stations consisted of a Güralp CMG-40T seismometer and a REF TEK 130 digitizer, with a sampling rate of 40 samples/s. These local Weston Observatory stations were run from 17 October until 12 November but only detected one aftershock (on 20 October).

Figure 2 shows the AIDA vertical-component seismograms of the only aftershock recorded, with *P*- and *S*-phases marked. Because the 3C array and the HDA 2 were not in place at the time of the event, those recordings are not relevant to the analysis reported in this paper.

MAINSHOCK AND AFTERSHOCK PARAMETERS

The M_w 4.0 Waterboro, Maine, earthquake's epicenter was reported by the Weston Observatory to be at 43.60 ± 0.007° N, 70.65 ± 0.007° W. This location used 221 stations, of which only one was within 100 km of the epicenter (i.e., Franklin Falls dam station FFD, 82.4 km from epicenter). The preferred focal depth for this event is 7.0 km, obtained from a regional moment tensor inversion (USGS, 2012). The focal mechanism determined by the USGS (2012) was that of a reverse-faulting event striking north-northwest–south-southeast with a minor strike-slip component, which is consistent with the region's east–west-oriented maximum horizontal stress direction (Ebel and Kafka, 1991; Zoback, 1992). Unfortunately, the aftershock that is the focus of this paper was not recorded by the New England Seismic Network operated by Weston Observatory, ruling out the application of relative location techniques that would allow us to improve the mainshock location. Although the epicenter of the mainshock lies near the surface trace of a thrust fault mapped by Osberg *et al.* (1985), a direct relationship of the earthquake to the fault is problematic given the depth of the event and the dip of the focal mechanism.

One of the objectives of this AIDA experiment was to assess the improvement in hypocenter location that can be attained from dense recording compared with more traditional aftershock studies. Here, we located the aftershock using various subsets of the AIDA Maine deployment: (1) all 43 AIDA stations that recorded the event (Fig. 1b), (2) the AIDA sparse (location) array only (diamonds in Fig. 1b), (3) a subset of AIDA location stations (circled diamonds in Fig. 1b), and (4) all 43 AIDA stations and the three Weston stations (Fig. 1b). Variations 2 and 3 are analogous to traditional

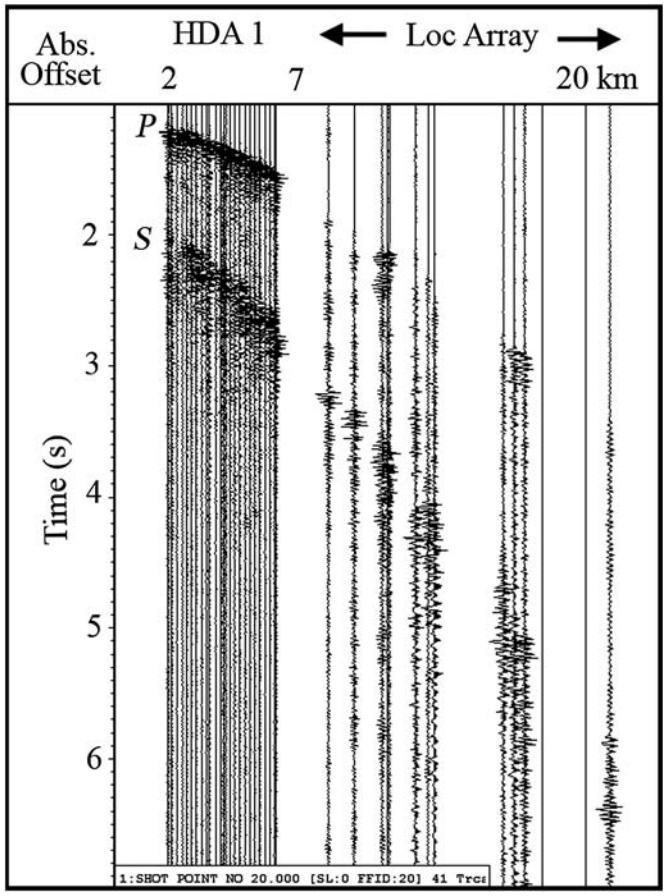

▲ **Figure 2.** Vertical-component seismograms of the 20 October aftershock, recorded by the 43 AIDA stations that were deployed at the time of the event. The horizontal axis is absolute offset from the epicenter. *P*- and *S*-arrivals are indicated in the figure. Event origin time has been time shifted to zero (zero time is off scale on the vertical axis) to replicate a controlled source record.

aftershock deployments, whereas variations 1 and 4 include the HDA (i.e., HDA 1).

All inversions for the hypocenter were done using the HYPOSAT earthquake location program (Schweitzer, 2001) and the regional *P*-wave velocity model of Luetgert *et al.* (1987). A V_P/V_S ratio of 1.73 (Luetgert *et al.*, 1987) was used to provide the *S*-wave velocity model for our locations.

Figure 3 presents the results for the hypocenter inversion using all four subsets of stations. As expected, the formal location errors shrink as more stations are used in the analysis. The largest errors for the inversion come from using variation 3, a subset of 11 AIDA location stations (Fig. 1b). A dramatic improvement occurs from variation 2 in which all 20 AIDA location stations were used. Further reduction in the uncertainty of the focal depth is observed when HDA 1 is included in the inversion (variation 1), which not surprisingly corresponds to the smallest location ellipsoid. The best hypocenter estimate is therefore at latitude 43.627 ± 0.001° N, longitude 70.684 ± 0.0014° W with a depth of 6.9 ± 0.15 km.

A very tangible benefit of using dense arrays such as HDA 1 is that it facilitates the estimation of a focal mechanism solution when using high-frequency sensors (i.e., geophones) in noisy environments (e.g., when deploying next to roads, as done in this study). The procedure to estimate the polarity of *P*-wave arrivals for the location array is illustrated in Figure 4. First, a band-pass filter (6–18 Hz) is applied to the HDA 1 seismograms (Fig. 4a), followed by a moveout correction to align the waveforms (Fig. 4b). Then, all the seismograms are added (stacked) to form a composite single trace (Fig. 4c). This master trace is then compared (i.e., visually and by cross correlation) with all location array stations to determine their polarity relative to the master trace derived from the dense array (Fig 4d). The last step in determining the focal mechanism solution is to identify location array stations with sufficiently high signal-to-noise ratios (SNRs) to allow robust *P*-wave first-motion determinations (e.g., Fig. 5). The resulting upper hemisphere focal mechanism indicates the aftershock was primarily a strike-slip event with nodal planes striking 37° and 300° and dipping 78° and 63°, respectively. In Figure 6, this focal mechanism is mapped onto a lower hemisphere projection to facilitate comparison with the mainshock focal mechanism obtained by the USGS (2012). Both focal mechanisms agree with the east–west direction of maximum horizontal stress for New England observed by Gephart and Forsyth (1985), Ebel and Kafka (1991), and Zoback (1992).

The coda length magnitude M_c of the aftershock recorded by the AIDA array is estimated from the Weston recordings to be M_c 0.6, based on the formula of Rosario (1979). Data presented by Ebel (1982) suggest that for New England M_c values equate to those of the Nuttli (1973) magnitude scale $m_g(L_g)$) in the $1.5 \le M_c \le 5$ range. Furthermore, it appears from the work of Street *et al.* (1975) that $m_g(L_g)$ magnitudes are consistent with the standard body-wave magnitude m_b for values in the eastern United States for earthquakes in the $0.5 \le m_b \le 3$ range. These relationships would suggest the body-wave magnitude of the AIDA recorded aftershock is about $m_b \sim 0.6$.

One of the advantages of dense array recording is that spatial coherence (i.e., visual trace-to-trace correlation) can result in the detection of smaller events than those generally identified from amplitude bursts within sparser arrays (Davenport *et al.*, 2015). If we conservatively assume that our AIDA array should be able to detect a coherent event down to an amplitude with SNR of ~1, we can estimate our event magnitude detection threshold by comparing the amplitude of the aftershock (i.e., magnitude $m_b \sim 0.6$) with the amplitude of the ambient background noise. Figure 7 shows amplitude versus time for the average seismic trace recorded with HDA 1. This plot indicates a difference of ~60 dB (i.e., amplitude ratio of 0.001) between the body waves (*P*- and *S*-waves) and the background noise. In Figure 8, we illustrate how a synthetic seismogram for the aftershock would appear on the dense array, assuming various levels of signal to noise. The added synthetic noise is Gaussian with a spectrum that is flat up to 50 Hz. The geometry of these gathers is the same geometry as that used in the deployment of HDA 1. In Figure 8, events with SNR ~1 are still

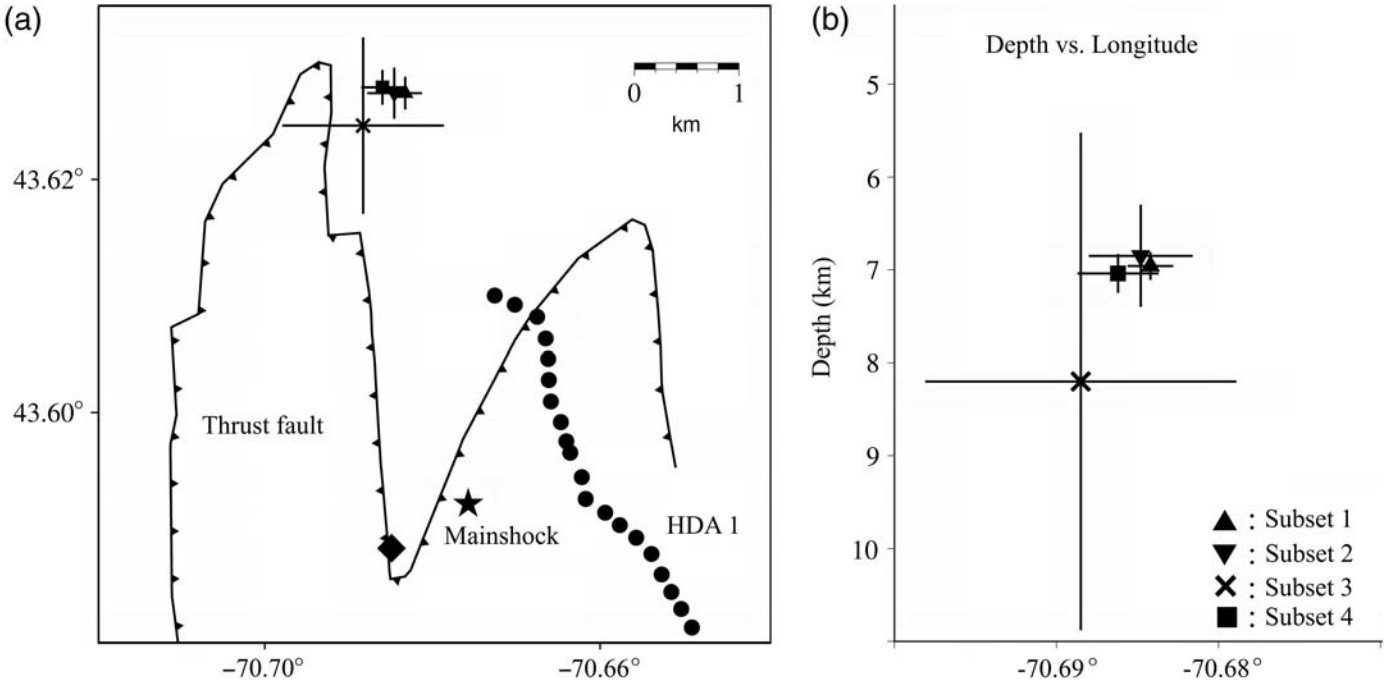

▲ **Figure 3.** Results for the aftershock hypocenter for the four subsets of stations with their corresponding error bars for the (left) epicenter and (right) depth. Subset 1 refers to all 43 AIDA stations that recorded the aftershock, subset 2 refers to all location stations, subset 3 refers to 11 AIDA location stations, and subset 4 refers to all 43 AIDA stations plus the three Weston stations (see Fig. 1b). The diamond in (a) corresponds to the only location array station falling within the map region. The thrust fault trace is shown (Osberg *et al.*, 1985).

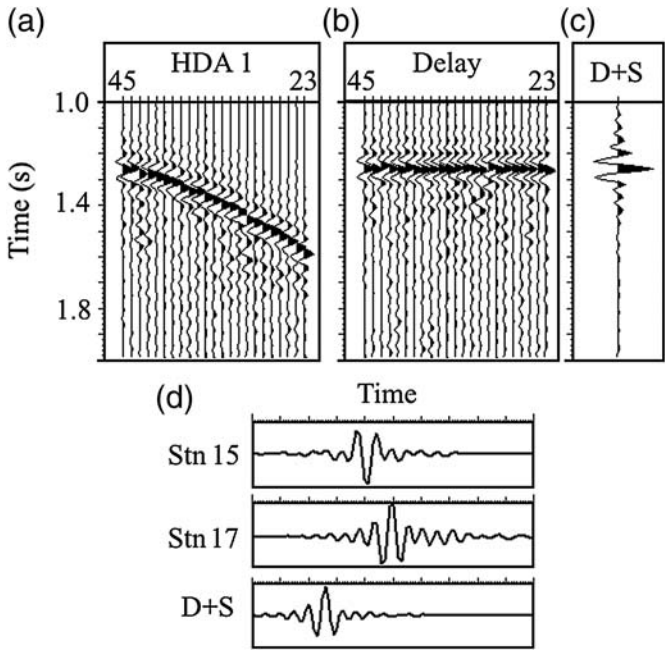

▲ **Figure 4.** (a) HDA 1 seismograms filtered (6–18 Hz) with clear moveout of *P*-wave arrivals. (b) HDA 1 seismograms *P*-wave arrivals corrected for the *P*-wave moveout. (c) Result of adding all seismograms in (b). (d) Polarity comparison between delay and sum trace (D + S) of HDA 1 and location array stations. Station 15 has opposite polarity to D + S, whereas station 17 has the same polarity as D + S.

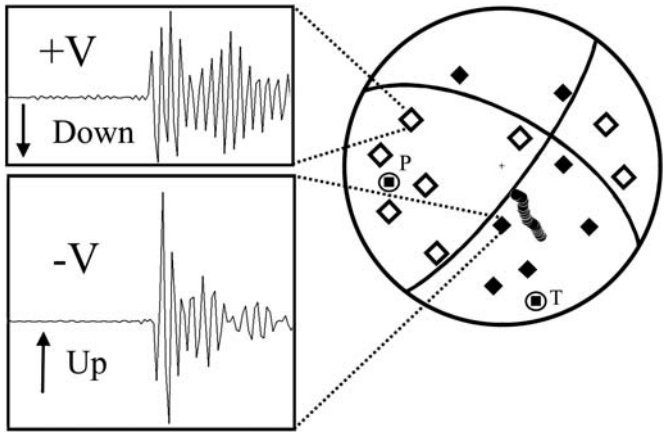

▲ **Figure 5.** Upper hemisphere focal mechanism for the Waterboro, Maine, aftershock. The circled squares indicate P- and T-axes. Diamonds and points indicate projections on the stereonet of stations used for focal mechanism solution (see Fig. 1). Filtered seismograms (12–40 Hz) of location array stations 1 and 17 are shown. Compression or upward ground motion (i.e., negative voltage, −V) is designated by filled symbols and downward motion by unfilled symbols.

clearly detectable by simple visual inspection, and much lower can be picked out if digital event detection (e.g., cross correlation) is applied. Extrapolating this result to the measured $m_b \sim 0.6$ aftershock amplitude with SNR = 60 dB,

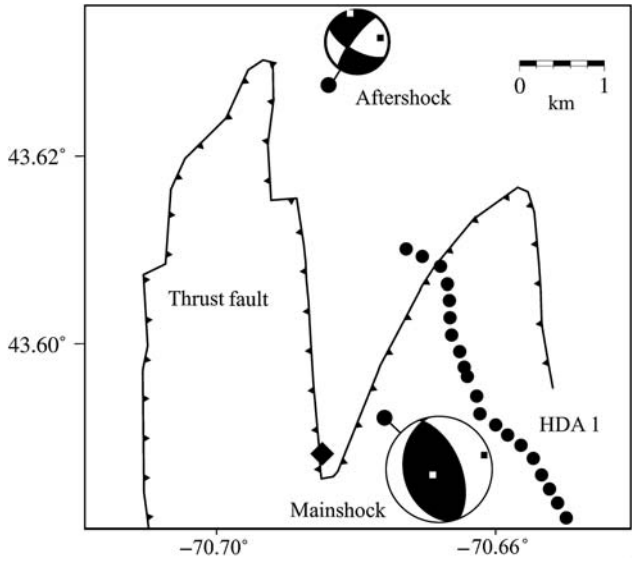

▲ **Figure 6.** Focal mechanisms on lower hemisphere projections for the 16 October mainshock and the 20 October aftershock. P and T axes are shown on each focal mechanism as black and white squares, respectively. The diamond corresponds to the only location array station falling within the map region. The thrust fault trace is shown (Osberg *et al.*, 1985).

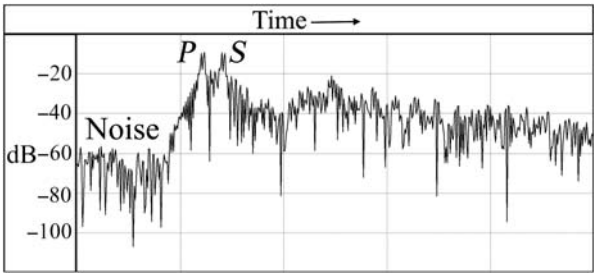

▲ **Figure 7.** Amplitude versus time plot of average seismogram recorded by HDA 1. Background noise, *P*- and *S*-arrivals are labeled.

we calculate that an $m_b - 2.5$ event would still have been obvious on the HDA 1 array recording.

IMAGING WITH EARTHQUAKE SOURCES

Given the depth of this event, correlating it to known faults at the surface is speculative at best. However, Quiros *et al.* (2012) demonstrate how AIDA arrays can potentially provide detailed reflection information on subsurface structure by using the aftershocks as imaging sources. Figure 9 explicitly illustrates

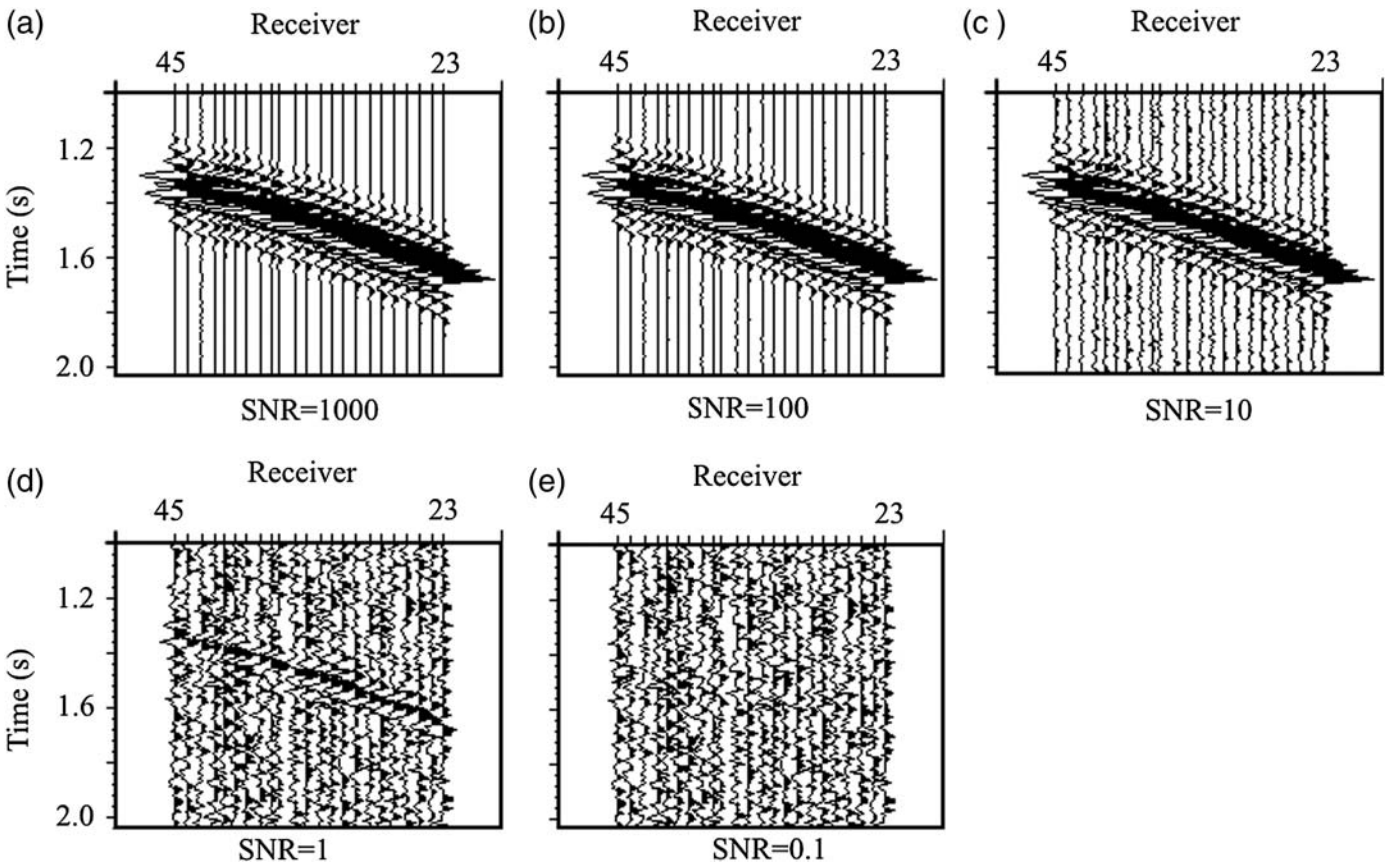

▲ **Figure 8.** Visual threshold estimation of HDA using the waveform from Figure 4c with a moveout derived from the aftershock *P* arrivals. Panels with different amounts of signal-to-noise ratio (SNR) of (a) 1000, (b) 100, (c) 10, (d) 1, and (e) 0.1. The horizontal axis displays offset identical to the geometry of the HDA 1 (i.e., ~200 m).

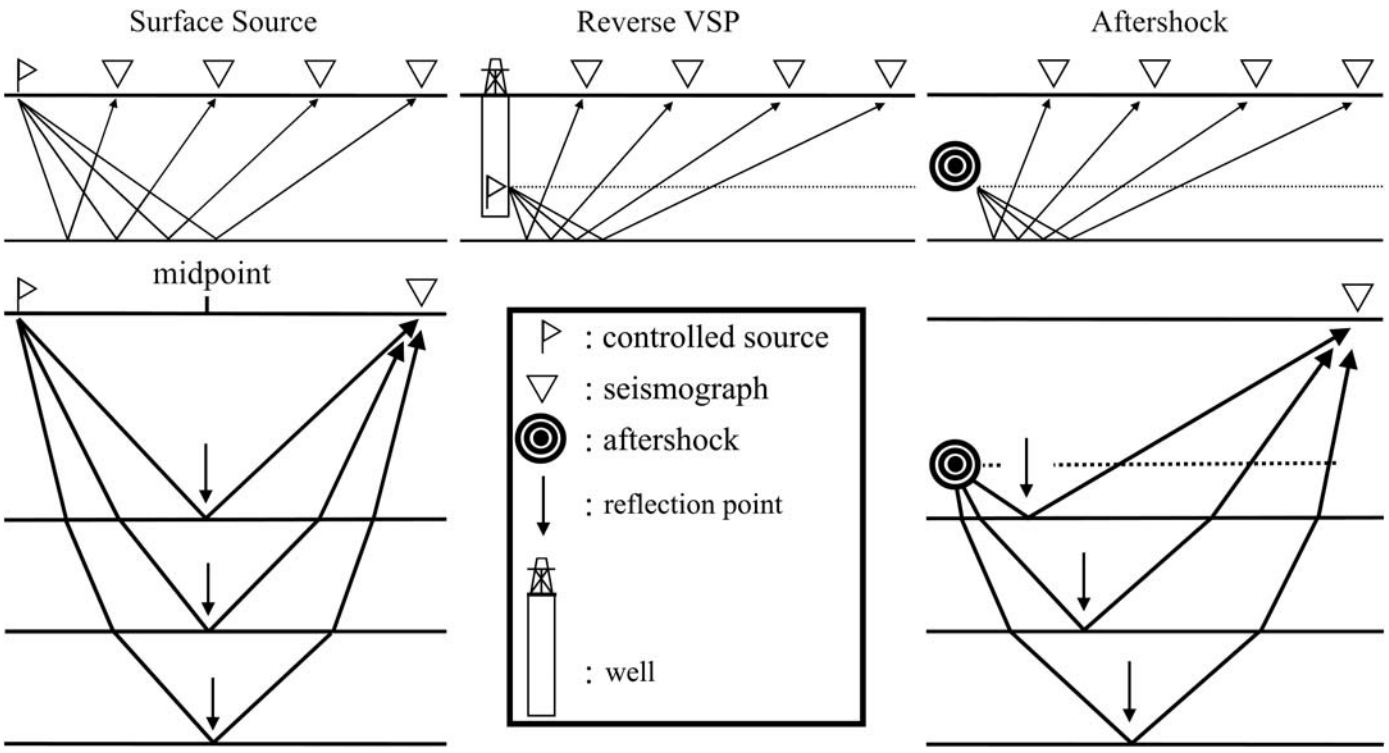

▲ **Figure 9.** (Top) Geometric difference between reflection ray paths for a surface source, for a subsurface artificial source in a conventional reverse vertical seismic profile (RVSP) survey, and for treating an aftershock as a reflection source. The differences of reflection point locations for a surface source–receiver pair (bottom left) and for an aftershock–receiver pair (bottom right). For a subsurface source (e.g., an aftershock), the reflection points move away from the source as a function of source hypocenter and receiver offset, resulting in curved seismograms in the space–travel time domain.

how aftershocks recorded by surface arrays can be treated as reverse vertical seismic profiles (RVSP). In this treatment, the earthquake serves as an illumination source for subsurface structure beneath the hypocenter. Although the true power of such an analysis is based on having multiple sources recorded by a dense 2D surface grid, even a single event recorded by a single dense surface profile can be used to generate a reflection profile in which geologic structures can be identified.

To calibrate our analysis, a synthetic vertical-component RVSP record was created with the exact geometry of the HDA 1 array and a simple explosive source at the aftershock hypocenter (Fig. 1b). Random noise with a root mean square amplitude equal to 2% of that of the artificial signal was added to the synthetic source trace. The synthetic record section was calculated using a simplified velocity model derived from controlled source, wide-angle data from central Maine (Luetgert *et al.*, 1987). The velocity model has two major assumed discontinuities beneath the hypocenter: a lower crustal reflector at 25 km and the Mohorovičić (Moho) discontinuity at 35 km. A VSP-to-common depth point (VSP–CDP) transformation (Hardage, 2000) is applied to the synthetic to obtain a single-fold reflection image beneath the source (Fig. 10a). This transformation consists of 3D point-to-point ray tracing for each source–receiver pair that correctly maps the lower crustal and Moho reflections into the horizontal distance–depth domain. Before applying the VSP–CDP transformation to the aftershock, the data went through a number of processing stages that are essentially identical to steps done in seismic reflection processing. These include first break picking, geometrical binning, static elevation correction, direct *S*-wave mutes (i.e., zeroed to avoid mapping it into the *P*-wave spatial domain), velocity-model improvement by least-squares inversion of travel times, and band-pass filtering (6–40 Hz).

Although the reflection image obtained by applying the VSP–CDP transformation to the processed aftershock (Fig. 10b) does not contain any particularly prominent reflections that could be interpreted as specific structures (e.g., faults or Moho), it does suggest a highly reflective lower crust in a manner similar to that observed on conventional deep seismic reflection images in the northern Appalachians (e.g., Spencer *et al.*, 1989).

CONCLUDING REMARKS

As expected, the availability of a large number of stations favorably distributed around an aftershock zone greatly improves hypocentral locations, especially if those stations are positioned at very close spacing, as well as providing sufficient data for source function (i.e., focal mechanism) recovery while using instrumentation designed for reflection seismology and deployed in noisy environments (i.e., next to roads). These benefits of this kind of deployment are expected for several

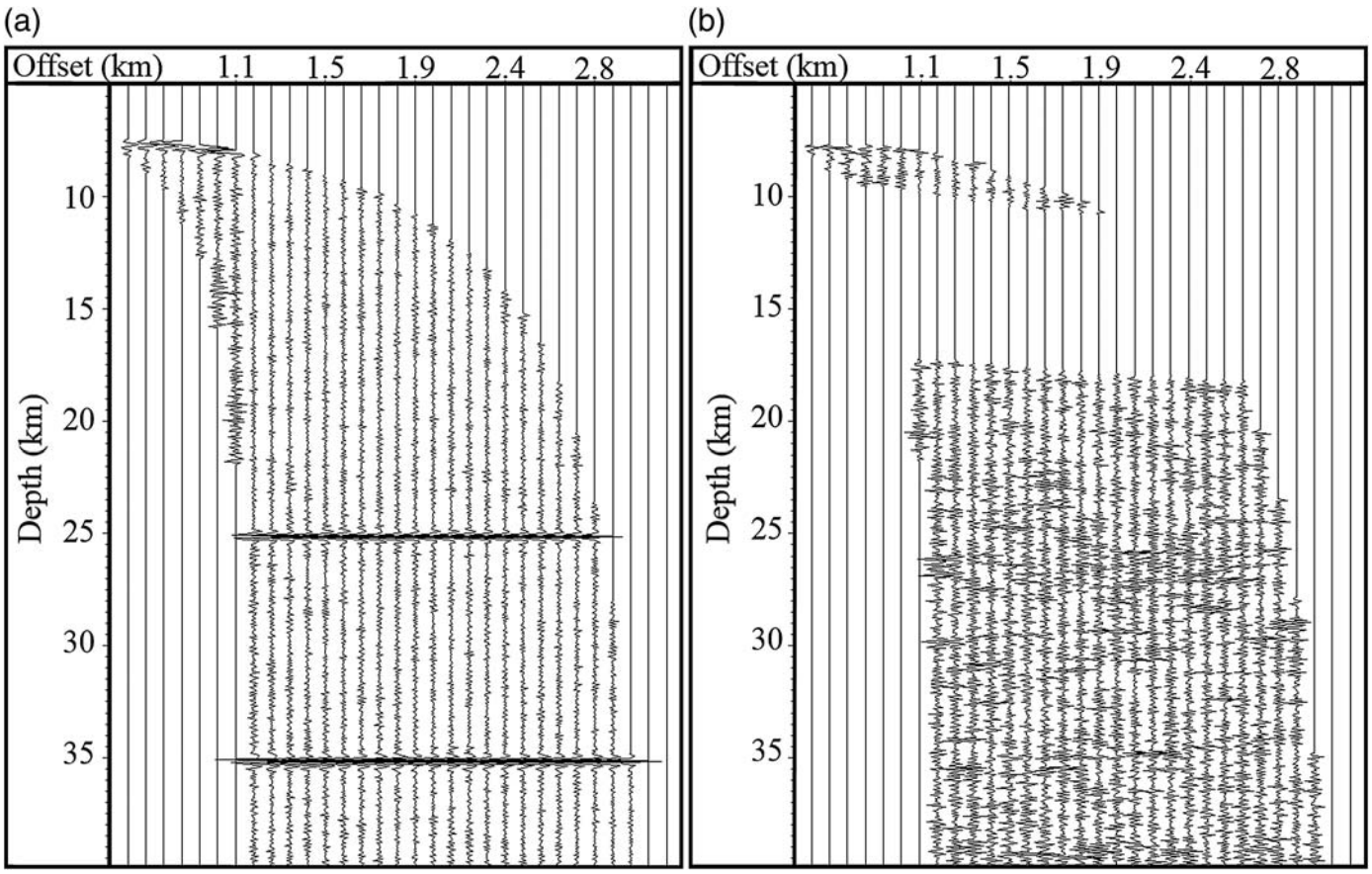

▲ **Figure 10.** Unmigrated 2D reflection image extracted from a 3D volume after the vertical seismic profiling–common depth point (VSP–CDP) transformation of (a) a vertical-component synthetic record with identical geometry to the Maine aftershock modeled with a 25 km deep reflector and a 35 km deep Moho discontinuity (2% noise added), and (b) the Maine aftershock vertical-component record with muted *S*-wave arrivals and exponential gain to equalized amplitudes.

reasons: the favorable azimuthal coverage, the large redundancy of the recordings, and, perhaps not least, to the fact that if enough stations are present, some are likely to be directly above the hypocenter and thus improve depth control immensely. Perhaps the most powerful aspect of this approach is that it can be applied to very small events that are well beyond the threshold of detection for conventional arrays. In this case, we believe the AIDA Maine deployment should have detected events as small as m_b approximately −2.4. The lack of such events underscores the small number of aftershocks previously noted for some earthquakes in New England (Ebel, 1984).

A novel aspect of dense arrays is that reflection imaging of subsurface structures can be achieved by treating earthquakes as sources in an RVSP geometry. Applying the VSP methodology (Hardage, 2000) to the only recorded aftershock in this experiment results in an unmigrated reflection image showing hints of lower crustal reflectivity reminiscent of continental reflection surveys throughout the Appalachians. If more aftershocks had been available and recorded by a true dense 2D surface array (i.e., grid of stations), a more useful image of the hypocentral volume would have been recovered.

Both the AIDA Virginia and AIDA Maine deployments were pilot studies using instrumentation that was available but designed for another purpose. However, state-of-the-art industry instrumentation is now available that would facilitate continuous recording for long intervals of time (i.e., 2–4 weeks) with 1000–10,000 highly portable 3C instruments. The Maine experiment makes clear that such recording should revolutionize our ability to characterize aftershocks distributions and image their related structures.

ACKNOWLEDGMENTS

The authors thank the National Science foundation (NSF) for funding the Aftershock Imaging with Dense Arrays (AIDA) Virginia and Maine experiments under the NSF grant EAR-215789, the Incorporated Research Institutions for Seismology Program for Array Seismic Studies of the Continental Lithosphere (IRIS–PASSCAL) team for their excellent technical support, Schlumberger for providing processing and modeling software (Vista 3D and OMNI 3D, respectively) and software support. Generic Mapping Tools (Wessel *et al.*, 2013), Vista

3D, and OMNI 3D were used to create the figures presented.

REFERENCES

Bounif, A., C. Dorbath, A. Ayadi, M. Meghraoui, H. Beldjoudi, N. Laouami, and M. Frogneux (2004). The 21 May 2003 Zemmouri (Algeria) earthquake M_w 6.8: Relocation and aftershock sequence analysis, *Geophys. Res. Lett.* **31**, L19606, doi: 10.1029/2004GL020586.

Brown, L. D., K. Davenport, D. A. Quiros, L. Han, C. Chen, J. A. Hole, R. B. Lohman, A. J. Ferguson, N. Fenning, W. D. Barnhart, *et al.* (2011). Aftershock Imaging with Dense Arrays (AIDA) following the August 23, 2011, M_w 5.8, Virginia earthquake: Feasibility demonstration and preliminary results, *Eos Trans. AGU* **1,** (Fall Meet.), Abstract S14B-06.

Davenport, K. K., J. A. Hole, D. A. Quiros, L. D. Brown, M. C. Chapman, L. Han, and W. D. Mooney (2015). Aftershock imaging using a dense seismometer array (AIDA) after the 2011 Mineral, Virginia, earthquake, in *The 2011 Mineral, Virginia, Earthquake, and Its Significance for Seismic Hazards in Eastern North America*, J. W. Horton Jr., M. C. Chapman, and R. A. Green (Editors), Geol. Soc. Am. Spec. Pap. 509, 1–283, doi: 10.1130/2015.2509(15).

Ebel, J. E. (1982). M_L measurements for northeastern United States earthquakes, *Bull. Seismol. Soc. Am.* **72,** 1367–1378.

Ebel, J. E. (1984). Statistical aspects of New England seismicity from 1975 to 1982 and implications for past and future earthquake activity, *Bull. Seismol. Soc. Am.* **74,** 1311–1329.

Ebel, J. E., and A. L. Kafka (1991). Earthquake activity in the northeastern United States, in *Neotectonics of North America*, D. B. Slemmons, E. R. Engdahl, M. D. Zoback, and D. D. Blackwell (Editors), Geological Society of America, 277–290, ISBN: 0813753066.

Gephart, J. W., and D. D. Forsyth (1985). On the state of stress in New England as determined from earthquake focal mechanisms, *Geology* **13,** 70–72.

Hardage, B. A. (2000). Vertical Seismic Profiling: Principles, in *: Handbook of Geophysical Exploration: Seismic Exploration*, K. Helbig and S. Treitel (Editors), Elsevier Science, Oxford, United Kingdom, ISBN: 0-08-043518-1.

Huang, Y., J. P. Wu, T. Z. Zhang, and D. N. Zhang (2008). Relocation of the M8.0 Wenchuan earthquake and its aftershock sequence, *Sci. China Earth Sci.* **51,** 1703–1711.

Kim, W. Y., and M. Chapman (2005). The 9 December 2003 central Virginia earthquake sequence: A compound earthquake in the central Virginia seismic zone, *Bull. Seismol.l Soc. Am.* **95,** 2428–2445.

Luetgert, J. H., C. E. Mann, and S. L. Klemperer (1987). Wide-angle deep crustal reflections in the northern Appalachians, *Geophys. J. Int.* **89,** 183–188.

Nuttli, O. W. (1973). Seismic wave attenuation and magnitude relations for eastern North America, *J. Geophys. Res.* **78,** no. 5, 876–885.

Osberg, P. H., A. M. Hussey, and G. M. Boone (1985). Bedrock geologic map of Maine, *Maine Geological Survey* scale 1 (500,000).

Quiros, D. A., L. D. Brown, K. Davenport, L. Han, J. A. Hole, M. C. Chapman, W. D. Mooney, and A. Cabolova (2012). Reflection imaging using RVSP processing of aftershock recordings from the August 23, 2011 central Virginia earthquake, *Eos Trans. AGU* **1,** (Fall Meet.), Abstracts 2461.

Rosario, M. A. (1979). A coda duration magnitude scale for the New England seismic network, *Master's Thesis in Geophysics*, Boston College, Massachusetts.

Schweitzer, J. (2001). HYPOSAT—An enhanced routine to locate seismic events, *Pure Appl. Geophys.* **158,** 277–289.

Spencer, C., A. Green, P. Morel-à-l'Huissier, B. Milkereit, J. Luetgert, D. Stewart, J. Unger, and J. Phillips (1989). The extension of Grenville basement beneath the northern Appalachians: Results from the Quebec-Maine seismic reflection and refraction surveys, *Tectonics* **8,** 677–696.

Street, R. L., R. B. Herrmann, and O. W. Nuttli (1975). Spectral characteristics of the Lg wave generated by central United States earthquakes, *Geophys. J. Int.* **41,** 51–63.

U.S. Geological Survey (USGS) (2012). *M 4.0-Maine (BETA), contributed moment tensor by USGS National Earthquake Information Center*, http://comcat.cr.usgs.gov/earthquakes/eventpage/pde20121016231223780_3#scientific_moment-tensor (last accessed February 2015).

Wessel, P., W. Smith, R. Scharroo, J. Luis, and F. Wobbe (2013). Generic Mapping Tools: Improved version released, *Eos Trans. AGU* **94,** 409–410.

Zoback, M. L. (1992). First- and second-order patterns of stress in the lithosphere: The World Stress Map Project, *J. Geophys. Res.* **97,** 11,703–11,728.

Diego A. Quiros
Anastasija Cabolova
Larry D. Brown
Chen Chen
Department of Earth and Atmospheric Sciences
Cornell University
112 Hollister Drive
Ithaca, New York 14853 U.S.A.
daq7@cornell.edu

John E. Ebel
Justin Starr
Weston Observatory
Department of Earth and Environmental Sciences
Boston College
381 Concord Road
Weston, Massachusetts 02493 U.S.A.

Published Online 25 March 2015